International Journal of Scientific Engineering and Applied Science (IJSEAS) – Volume-7, Issue-3, March2021
ISSN: 2395-3470
www.ijseas.com

Analysis Of The Electric Contact Closure Through The Finite Element Method Using The Vibration Of Reversed Vertical Disconnect Switches

Maira Andréia Luckmann Mores[1], Agenor Dias de Meira Junior[2], Charles Leonardo Israel[3] Márcio Walber[4]

[1] University of Passo Fundo, Passo Fundo, Brazil

[2] University of Passo Fundo, Passo Fundo, Brazil

[3] University of Passo Fundo, Passo Fundo, Brazil

[4] University of Passo Fundo, Passo Fundo, Brazil

Abstract

The disconnector is a switching device used to connect/disconnect an electrical circuit at the substation and to protect the system, with automatic and remote activation. Often, the closing maneuver is not completed. This work evaluates the use of vibration to remotely complete the closing of electrical contacts by means of vibration generated through a vibrator. The vibration produced by this device is transmitted to the main contacts through the structure of the disconnector, promoting its closure. The purpose of the analyses was to determine the frequencies, amplitudes, and excitation times that conclude the closing of the electrical contact of the disconnector and the values of the stresses produced on the structure and the mechanical components of the disconnector. This work presents a numerical model of the reverse vertical disconnector, the materials that compose it, the boundary conditions applied and the limitations of the model and how to circumvent them. The following shows the calibration of the model and the experimental and finite element method (FEM) determination of the natural frequencies of the structure. It presents dynamic simulations using FEM and implicit analysis through the Ls-dyna software, with excitation frequencies of 5 Hz, 10 Hz, 20 Hz, 40 Hz, and 80 Hz, for prescribed displacement amplitudes up to 3 mm, determining the displacements generated in the electrical contacts, the time to reach the closure of the electrical contacts, the stresses in the insulators, main blade, and mobile and fixed contact, and the effect of vibration on the disconnecting twisting moment of the switch. The analyses show that excitation frequencies of 5 Hz, 10 Hz, and 20 Hz and the displacement amplitude prescribed in the base of up to 3 mm produce the effect of completing the closing of the electrical contacts, without great impact on the electrical contacts, as well as the generation of stress values on the disconnector within safety limits.

Keywords: *Author Guide, Article, Camera-Ready Format, Paper Specifications, Paper Submission.*

1. Introduction and contextualization

The point of protection, control, transmission, and distribution of high-power energy from the generating source to the consumer is called a substation. The disconnector is the equipment responsible for connecting the electrical circuit and protecting the system in the substation. The disconnectors are positioned at a high height to avoid the risk of accidents, and their operation is controlled remotely. When it is activated remotely to close the electrical contact, closing often does not happen, requiring the presence of an operator on site to complete the closing of the contacts manually, with the help of a stick.

The difficulties of operating the disconnector at a distance is the subject of research in Rocha's dissertation [1], where the use of a unidirectional electromechanical vibration motor fixed to the base of the disconnector structure is described, which, when vibrating, closes the main contacts. Rocha [1] performed experiments for a

horizontal double side opening disconnector, proving the efficiency of the vibration effect for closing the electrical contacts, which resulted in Brazil/South patent No. BR 1020130201987 [2].

This work evaluates the effect of vibration on the disconnection of switches of another constructive type (230 kV monopolar reverse vertical disconnector), as proposed by Rocha [1], through dynamic analysis using the finite element method (FEM) under the action of vibration generated by a motovibrator, determining the frequency, amplitude, and time required to close the electrical contacts and the stress values produced on the structure and the mechanical components of the disconnector.

The company CEEE (State Electricity Company) financed this work. For this purpose, the company installed a reverse vertical disconnector on the Passo Fundo University Campus (UPF), UPF Science and Technology Park, which is the object of this work.

1.1 Research method and study organization

The research carried out in this work consisted of dynamic analysis to determine the frequency and activation time of the vibrator that would produce the closing of the contacts and determination of the maximum displacement amplitude from the base of the structure (C profiles) that could be generated by the motovibrator action and the stresses produced in the mechanical and structural components.

The article is organized into the following sections. Section 2 presents a literature review of the reverse vertical disconnector, a dynamic analysis, and on explicit and implicit time integration algorithms. Section 3 presents the numerical model of the reverse vertical disconnector, the materials that compose it, the boundary conditions applied and the limitations of the model and how to overcome them. Section 4 shows the calibration of the model and the experimental and FEM determination of the natural structure frequencies. Section 5 presents dynamic simulations with excitation frequencies of 5 Hz, 10 Hz, 20 Hz, 40 Hz, and 80 Hz, determining the displacements generated in the electrical contacts, the time to reach the closing of the electrical contacts, the stresses in the insulators, blade main, and mobile and fixed contact, and the effect of vibration on the twisting moment of the disconnector. Finally, in section 6, the conclusions of the article are presented.

2. Theoretical basis

2.1 Disconnectors

The disconnect switch is a maneuvering device used in the electrical system, and it performs the following functions: interconnection of generators, transformers, and transmission lines [3], allowing continuity of the electrical circuit; isolation of the components of the substations so that their maintenance is carried out; performance of electrical power flow transfer maneuvers; and system protection.

Systems capable of verifying the correct opening and closing operation of high voltage disconnectors of power substations were presented by Carrasco and Lambert-Torres [4], who presented a digital analysis of the torque curve provided by the drive motor during the disconnector maneuvers, monitoring the contact of the active part of the disconnector.

Mosalam and Günay [5] presented the development and validation of a hybrid simulation system in real time for dynamic tests of high voltage vertical disconnect switches. The system consisted of a computational model of the support structure, a physical model of the insulator column, a controller, a data acquisition system, and a digital signal processor.

Mosalam and Günay [6] presented the results of a parametric study that consisted of real-time hybrid simulation tests of electrical insulator poles and evaluation of the effect of the damping and stiffness of the support structure on the response of the disconnecting switches with two different insulating materials, porcelain and polymer, presenting typical natural frequencies and damping rates.

Semedo et al. [7] presented a standalone, wireless, multivariate intelligent sensor to collect, validate, and locally process position alignment and temperature data on remotely operated high-voltage disconnectors as part of an instrumentation system that provides data for active management systems applied to intelligent power grid substations.

Zangl et al. [8] stated that for the transmission of electricity, high voltage overhead lines play an important role because energy transmission costs are comparatively low and with online monitoring of power line conditions critical states can be detected in advance and appropriate countermeasures can be applied. Thus, they demonstrated devices that could monitor a conductor.

Galin et al. [9] presented the results of systematic measurements of an electromagnetic field carried out in high and very high voltage substations of the Romanian electric grid in order to meet the requirements of the European Union guidelines regarding human exposure to electromagnetic fields. Results for a 400/220 kV substation and two 110/20/10 kV substations were presented.

According to the ABNT (Brazilian Association of Technical Standards) NBR 7571 standard [10], the disconnectors are classified as in vertical operation when the mobile contact moves in a plane normal to the base plane [3]. They are called reverse vertical (RV) when they are composed of insulating columns that support the mobile contact set and one of them activates the set, and it also consists of an upper fixed contact where the coupling occurs [Figure 1(a)]. The disconnector operates from an opening or closing command that is given from a button on the control panel. The motor is energized and starts to rotate, moving its axis. The shaft is coupled to a gearbox that turns a worm gear speed reducer, and this, in turn, will cause the movement of the transmission shaft that rotates the blade mechanism assembly, located above the insulating column, thus moving the main blade and opening or closing the disconnector [11]. The equipment consisted of the following structure [Figure 1(b)]: 1) the sub-base metal structure, 2) the C-section disconnector base, 3) the fixed insulating columns in cast iron and porcelain, 4) the mobile insulating column, 5) the main blade drive, 6) the main blade or mobile contact, and 7) the fixed contact.

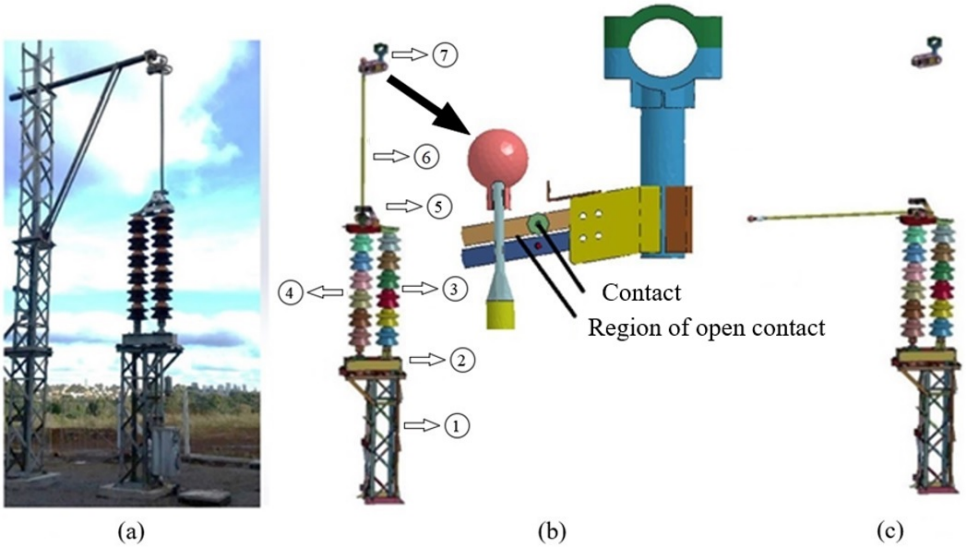

Figure 1. (a) Reverse vertical disconnector, (b) closed 3D model, and (c) open 3D model.

The disconnect switch can be operated manually or it can be motorized [11]. Figure 1(b–c) shows the reverse vertical disconnector in the closed and open position, respectively. The normal working mode of the disconnector is in the closed position when there is electrical current transmitted through the main or electrical contacts [12]. Often, after remote activation of the reverser, the electrical contact does not close, as shown in detail in Figure 1(b). In this situation, the reopening of the disconnector is commanded, and its closure is attempted again. If complete closure has not yet occurred, the operator moves to the location where the disconnector is located, and with an isolated maneuver stick, pushes the mobile contact to the correct position.

When the electrical contact is not made, voltaic arc, wear and oxidation occur [13], which further impair the closing effect and reduce the equipment service life.

2.2 Dynamic analysis

A dynamic system consists of a set of elements that have mass and that are capable of relative movements [14]. Due to the variation in speed that occurs during the movements and since the elements do not have negligible mass or inertia [15], as well as the application of external forces, the kinetic energy of the system can vary with time [16]. For the analysis of a dynamic system using FEM, discretization can be used to determine the displacements of a limited number of parameters associated with the structure's nodes. Each of these parameters is called a degree of freedom [17].

Equation (1) represents the dynamic behavior of a structure with varying degrees of freedom [18], as follows:

$$[M].\{\ddot{U}\} + [C].\{\dot{U}\} + [K].\{U\} = \{F(t)\} \qquad (1)$$

where $[M]$ is the matrix that counts the masses, $\{\ddot{U}\}$ is the column matrix that contains the accelerations, $[C]$ is the damping matrix, $\{\dot{U}\}$ is the column matrix of velocities, $[K]$ is the stiffness matrix of the structure, $\{U\}$ is the column matrix of displacements, and $\{F(t)\}$ is the column matrix of the forces. To solve Equation (1), explicit and implicit methods can be used [19].

2.2 Explicit and implicit methods

Note that Equation (1) is a time-dependent equation. The methods of direct temporal integration (also called simply direct methods) consist of solving equation (1) in discrete times. A certain variation in displacements, speeds, and accelerations is assumed in the interval between one time and another. The form of this hypothesis will determine the precision and stability of the method [20].

For non-linear problems, only numerical solutions are possible. Explicit methods, such as the central differences method, are the most used. For explicit methods, the equation of motion is calculated in the previous time step, t_n, while implicit methods use the motion equation for the new time step, t_{n+1} [21].

The implicit and explicit terms refer to time integration algorithms. In the explicit method, internal and external forces are added for each nodal point, and the nodal acceleration is calculated by dividing by the nodal mass. The solution is achieved by integrating this acceleration into time. The maximum timestep size is limited by courant's condition [22], producing an algorithm that typically requires many relatively non-time-consuming steps. Explicit analysis is suitable for dynamic simulations such as impact and crash, but it becomes prohibitive and time-consuming for long-term events or static analysis.

In the implicit method, a global stiffness matrix is calculated, inverted, and applied to the unbalanced force balance to obtain an increment in displacement. The advantage of this method is that the timestep size can be selected by the user. The disadvantage is the large numerical effort required to store and factor the stiffness

matrix. Implicit simulations, therefore, typically involve a relatively small number of time steps of high computational cost [23].

An implicit analysis can be linear or non-linear. It is also used to perform an eigenvalue analysis to extract frequencies and modal shapes.

A nonlinear implicit simulation is typically divided into several steps. In a dynamic simulation, these are the time steps. Multiple time steps can be used to divide the nonlinear behavior into manageable parts, to obtain results in intermediate stages during the simulation, or possibly to solve a particular frequency of movement in a dynamic simulation. At each time step, an equilibrium geometry is sought with internal and external force balances in the model. A nonlinear equation solver performs an interactive search using one of several methods based on Newton's method. The convergence of these interactive processes is achieved when the displacement and/or energy norm falls below the tolerances prescribed by the user. Within each equilibrium iteration, a linear system of shape equations (equation 2) needs to be resolved. To do this, the stiffness matrix, K, is inverted and applied to the external equilibrium balance or R residue, producing an incremental displacement, Δu. Storing and resolving this linear system requires a large amount of CPU memory, which increases the cost of implicit analysis.

$$K\Delta u=R \qquad (2)$$

Different procedures for solving nonlinear equations are available to find equilibrium within each time step [24]. All are iterative in nature [25]. In the full Newton method, a new stiffness matrix is formed and inverted at each equilibrium iteration. This is the most time-consuming method, but it may require few iterations to reach equilibrium.

In the modified Newton method, several iterations are performed using the same stiffness matrix. After each iteration, the geometry is updated using Δu and the new R is calculated. This approach reduces time by avoiding some formations and factorization of the K stiffness matrix, but it usually requires more iterations to reach equilibrium.

Another method that can be used is the quasi-Newton method. In this method, the inverted K matrix is used for several iterations, but it is improved after each iteration. If convergence is not achieved after 10 iterations or if divergence is detected, then a new stiffness matrix is automatically formed and inverted. The method takes the name of BFGS update and is given by equation (3) [19], as follows:

$$K_{n+1}^{-1} = (I + wv^T)K_n^{-1}(I + vw^T) \qquad (3)$$

where a new stiffness matrix inverse (K_{n+1}^{-1}) is approximated by the old stiffness matrix inverse (K_n^{-1}), and the outer product of two carefully chosen vectors *v* and *w* [19]. The BFGS method also allows the option to choose the full Newton method.

3. Numerical model of the reverse vertical disconnector

Reverse engineering [26] is used for 3D modelling of the reverse vertical disconnector (Figure 1) [27] using a creaform portable 3D scanner, HandySCAN 3D model (accuracy of up to 0.03 mm), and VX Elements software for data acquisition and analysis of acquired information.

Table 1 indicates the density and elasticity modulus values and the Poisson's ratio of each material of the disconnector, modelled as plastic kinematic or rigid.

Table 1: List of disconnector materials with their respective mechanical properties.

Material	*Density* (kg/m^3)	*Modulus of elasticity* (GPa)	*Poisson's ratio*	*Localization*
Carbon steel	7.850	200	0.3	Sub-base, base, and some parts of the blade mechanism
Cast iron	7.200	110	0.28	Internal part of the insulating columns and parts of the blade mechanism and fixed contact
Copper	8.300	110	0.34	Movable and fixed contact plates and main blade
Aluminium	2.770	71	0.33	Anti-corrosion ring and main blade sphere
Porcelain	3.200	230	0.24	Skirt the insulating columns
Nylon	1.140	3	0.4	Fixed contact stop

Due to the complexity of the model, simplifications were carried out in order to reduce the computational effort for the simulation [Figure 2(a–e)]. Bearings were replaced with cylindrical joints, and springs were removed. Screwed joints were simulated through bonded contact, obtained through keywords and commands from the Ansys Workbench Ls-dyna software.

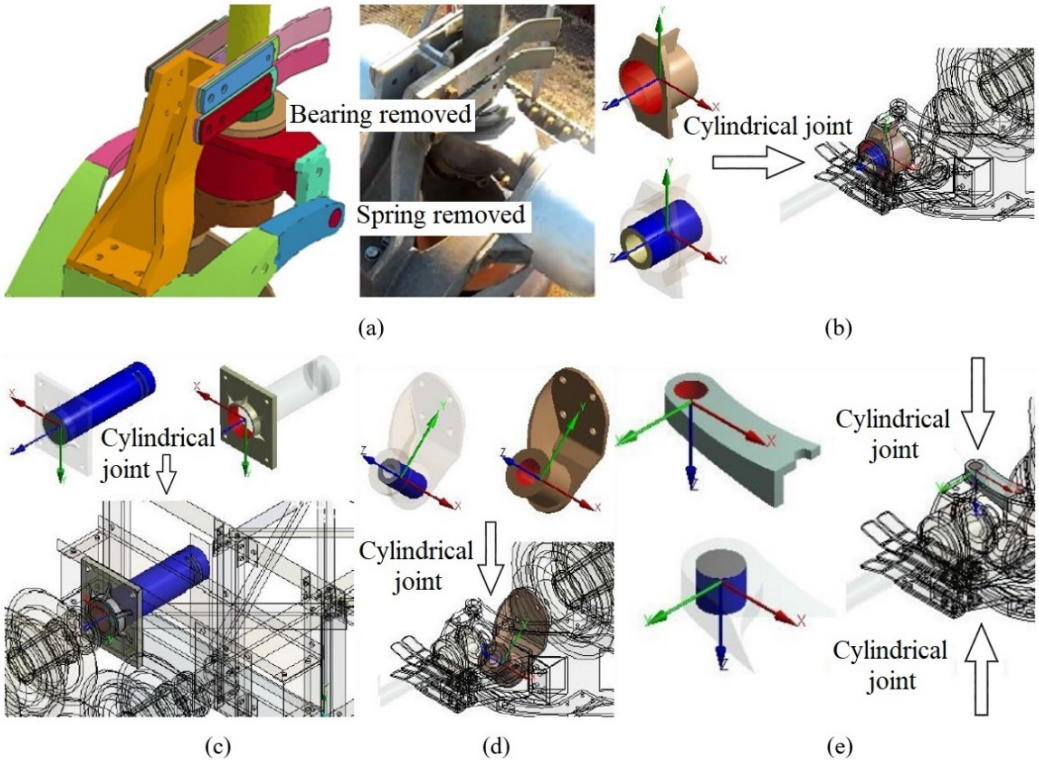

Figure 2. Simplifications in the model.

Four C profiles of the sub-base had their translation and rotation impeded in the x, y, and z directions [Figure 3(a), blue]. The fixed contact, which is suspended by an external structure, prevents rotation and translation in the x, y, and z directions [Figure 3(b), blue].

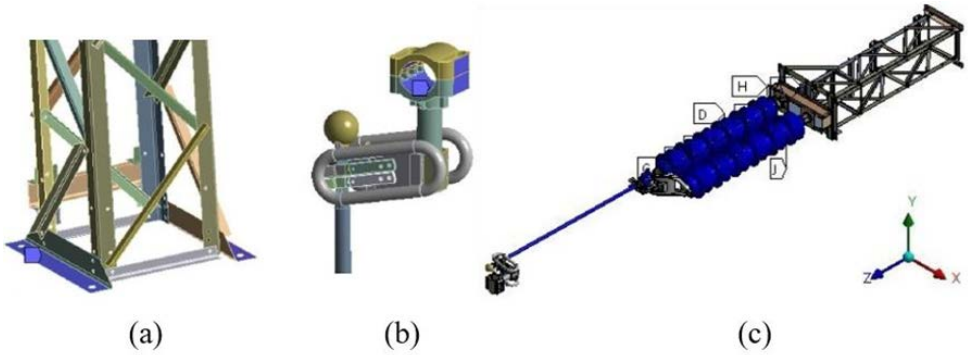

Figure 3. Boundary conditions.

When the main blade is activated in the real structure, the insulating columns tend to undergo a lateral movement in the *y* direction. This effect also appears in the implicit analysis performed, causing a non-centralized movement and shift to the lateral side of the main blade, and it also impairs the search for convergence and balance in each step of the implicit analysis. Even when reducing the time step size, this effect is not eliminated. To circumvent this problem, restrictions were applied to the components of the insulating columns and to the other elements of movement transmission in the transverse y direction [Figure 3(c), blue].

The thicknesses of the laminated profiles are 5 mm, 7 mm, and 10 mm (Figure 4). The profiles that are not indicated have a thickness of 5 mm.

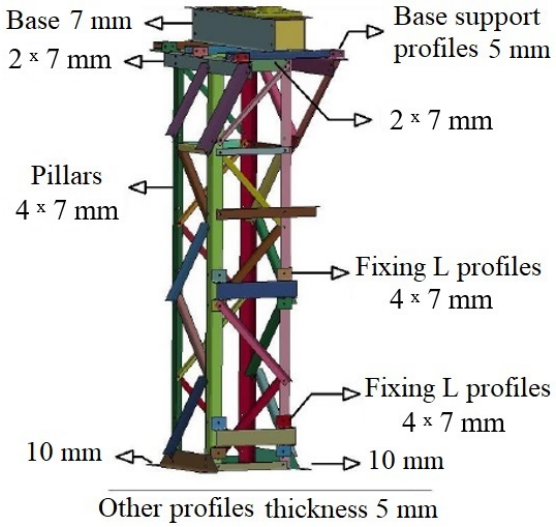

Figure 4. Sub-base.

The mesh was generated by the Ansys Workbench Ls-dyna software. Ls-dyna standard elements are highly efficient and use a single integration point. For implicit analysis, the use of more expensive formulations that are less susceptible to hourglass instability is generally more effective. The formulation of the shell element used was number 1 (Hughes-Liu), number 2 (Belytschko-Tsay), and number 6 (S/R Hughes-Liu), with four nodes. All of these elements include membrane deformations, bending, and shearing.

The Belytschko-Tsay formulation is the most economical and should be used unless some particular characteristic is required in the analysis. Hughes-Liu's formulation can work with the offset semi-plane. Hughes-Liu's co-rotational S/R formulation is fully integrated, so deformations due to the hourglass effect [28]

do not occur, but the computational cost is higher. The term hourglass means mesh instability and can also be called singularly spurious mode, a mechanism, a kinematic mode, or a zero-energy mode. The term hourglass refers to a nodal displacement vector that is not a rigid body movement, but nevertheless produces a zero-deformation energy state. This instability produces flaws in the element formulation process, similar to what occurs when using a low order Gauss square rule [21].

Solid components with similar dimensions, which cannot be represented by a shell, are discretized using solid elements with a formulation number of 10 (tetrahedron with an integration point) and formulation number of 2 (solid S/R with complete integration). They are solid elements of eight nodes that, by default, use an integration point. The mesh was generated with 841,746 nodes and 245,439 elements.

4. Calibration of the reverse vertical disconnector model

The methodology used for the calibration of the numerical model consisted of the following: 1) determination of the expected twisting moment values, 2) qualitative evaluation of the movements and cinematism, 3) quantitative evaluation and model calibration, and 4) experimental and numerical determination of the structure's natural frequencies.

4.1 Determination of expected twisting moment values

The weight of the copper tube was 19.4 kg, and the weight of the tip and ball at the end was 2.5 kg. The twisting moment obtained in relation to the turning point was 355.64 Nm (Figure 5), which is the minimum value for moving the main blade or movable contact.

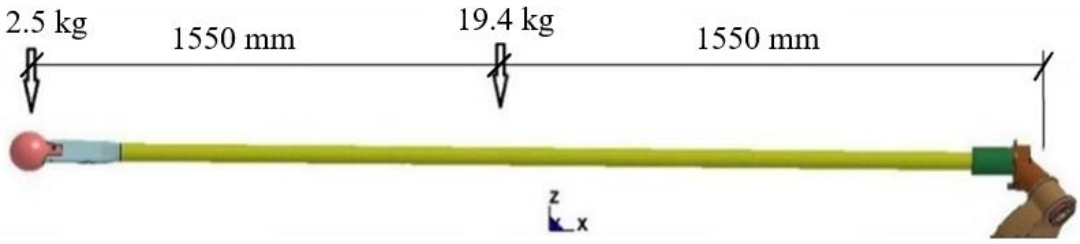

Figure 5. Simplified model of the main blade or movable contact.

Equation (4) determines the maximum available twisting moment for the motor shaft drive gearbox (1,664 Nm), where power, P, is 0.5 CV, rotation, N, is 950 rpm, the reduction is 450 times, T is the torque, and ω is the angular velocity.

$$T = P/\omega = P/(2\pi N) \qquad (4)$$

The order of magnitude of the expected twisting moment should be a value between 355.64 Nm and 1,664 Nm and is a reference for FEM calibration.

4.2 Qualitative evaluation of movements and cinematism

With a chamber of 24 positions per second, it was observed that the time required for uncoupling the main blade was 1.475 s. The time for the closing movement of the main blade was 2.175 s. The total time to uncouple and couple was 3.65 s. These times are for effective movement, it does not consider the time to reset the movements due to the end of stroke impact of the main blade.

Figure 6 shows a comparison of the decoupling movement of the FEM model and the real reverse vertical disconnector at 0 s, 0.26 s, 0.54 s, 1.05 s, and 1.5 s. It was observed that the FEM model reproduced the real movement.

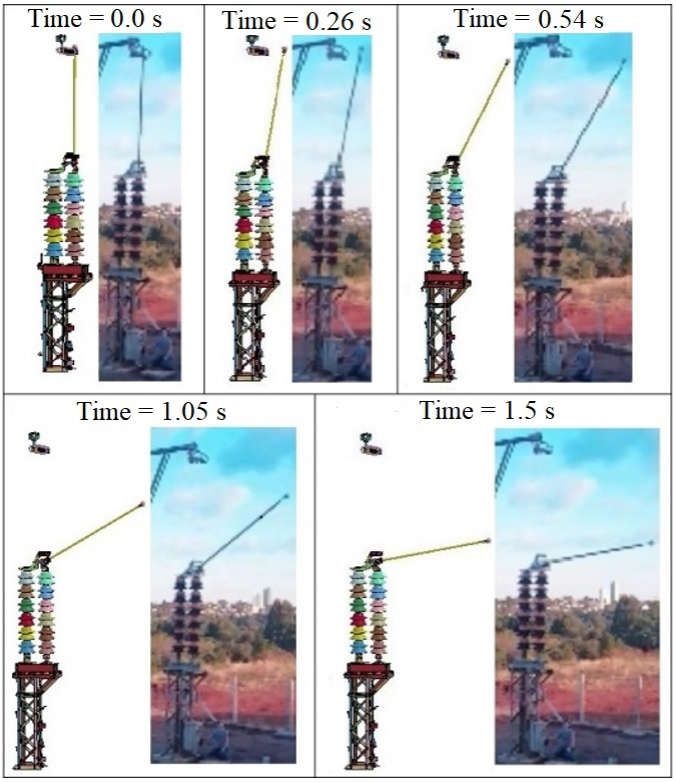

Figure 6. Uncoupling movement of the main blade and the moving contact (FEM × Real).

Figure 7 (a–b) shows two views of the main blade drive mechanism, comparing the movement of the main blade drive mechanism in the FEM model and the real reverse vertical disconnector, in the time of 0.0 s and 1.55 s, respectively. It appears that there is a good approximation of times and movements for the FEM model and the equipment.

Figure 7. Main blade drive mechanism.

4.3 Quantitative evaluation and model calibration

4.3.1 Control parameters used in dynamic simulation

The analysis is implicit using the ANSYS Ls-dyna software. Nonlinear analysis with standard BFGS update with full Newton nonlinear solution method to form a new stiffness matrix at each iteration was selected in the implicit solution control parameters. The solver used was the parallel multi-frontal sparse solver (SMP) standard to obtain the inverse of the global stiffness matrix. The parameters for automatic time-step control during implicit analysis were activated. The implicit dynamic control parameter was triggered for modal superposition analysis.

4.3.2 Control parameters used in model calibration

As the model of the vertical upright disconnector was built from reverse engineering by scanning/measuring its components, there were many imperfections in the model geometry that hindered the analysis, generating initial penetrations (presented as warnings in the message file generated by the program) between the parts that make up the structure and the movement transmission mechanisms. To solve these problems, it is necessary to adjust the control parameters related to the contacts between the component parts [19]. The function of the contacts is to allow the elements to interact with each other. In this way, these elements consider parts that impact, push, slide, or rub or parts that should be tied together. One way to characterize a contact algorithm is the penetration search method [19], which is the method used by the computational algorithm. The contact for iteration between bodies and parts used was automatic contact from surface to surface with definition of the static and dynamic friction coefficient.

To reduce the severity of the initial contacts, the scale factor for sliding contact penalty can be decreased. Another important factor is to define that the program ignores initial penetrations for the automatic contact options, which was the case in this work. The term "initial penetrations" refers to the first-time step in which the penetration is found. The modified default values apply to all contacts, but the contact parameters provided in each individual contact command will always take precedence over these defaults for that specific contact.

4.3.3 FEM model calibration

In the first step for model calibration, the twisting moment provided by the driving shaft was used, as shown in section 4.1. The scale factor for sliding contact penalty was adjusted so that the twisting moment value required for coupling/uncoupling the main blade was within the expected range.

For the second calibration step, another control factor is used. The stresses originate from another type of load applied in the same model of the disconnector with the same control parameters, generating a second analysis.

For the third step, for comparison, another analysis of a simple component of the disconnector structure is generated with boundary conditions taken from the model of the second analysis, thus obtaining a calibration check value. If the stress values obtained in the second and third stages are approximate, the disconnector model is considered, from the point of view of numerical analysis, calibrated.

4.3.3.1 First step: calibration through twisting moment

To simulate the closing and opening movement of the of the reverse vertical disconnector, rotations are prescribed on the driving axis and the blade mechanism axis, as shown in Figure 8.

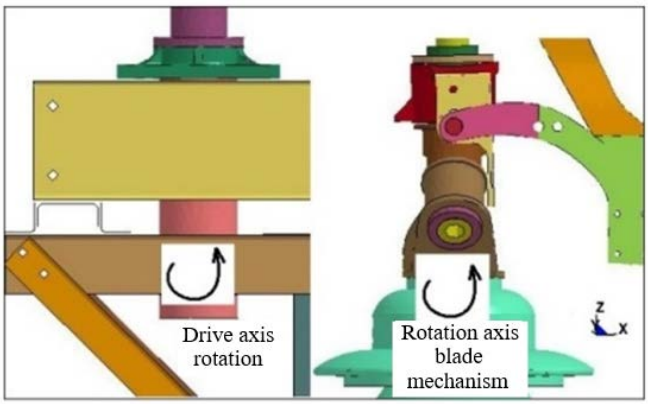

Figure 8. Prescribed rotation.

A rotation of 0.88 radians was prescribed on the driving axis in a time of 1.475 s for opening the main blade. To close it, 1.08 radians were prescribed in a time of 2.175 s. For the axis of the blade mechanism, 1.48 radians were prescribed for opening the main blade in a time of 1.475 s. To close it, 1.58 radians were prescribed in a time of 2.525 s, considering the total event time of 4.0 s. The values of the prescribed times and rotation were estimated through the video generated of opening and closing the real reverse vertical disconnector, seeking to approximate the actual movement behavior of the disconnector.

To calibrate the FEM model, the scale factor for sliding contact penalty (values between 0 and 0.1) was varied until obtaining values for the twisting moment that were verified during the opening and closing event of the main blade within the calculated limits of the twisting moment (section 4.1).
Figure 9 shows the opening movement of the main blade and the moving contact for times t = 1.475 s, 0.75 s, and 0.0 s and the closing movement of the main blade and moving contact for times t = 2.05 s, 3.0 s, and 3.65 s. The total processing time was 4.0 s.

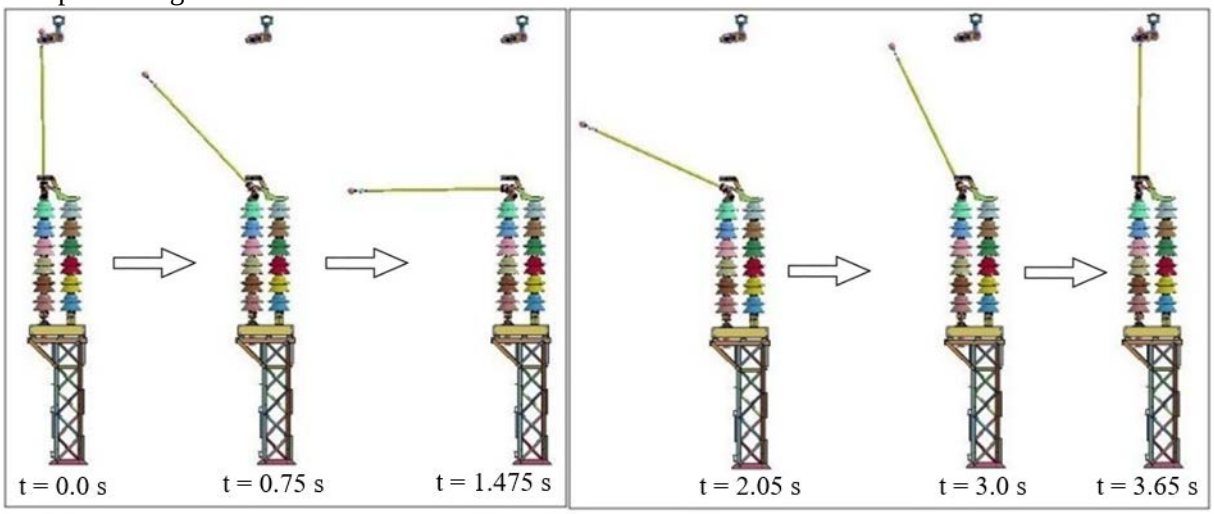

Figure 9. Opening and closing movement of the main blade and the movable contact.

The total twisting moment required to perform the prescribed rotations was obtained by adding the module of the twisting moments on both axes (Figure 8) shown in Figure 10. It is observed that the maximum twisting moment of the event is 918 Nm and occurs at 0.815 s, which is within the limits defined in section 4.1.

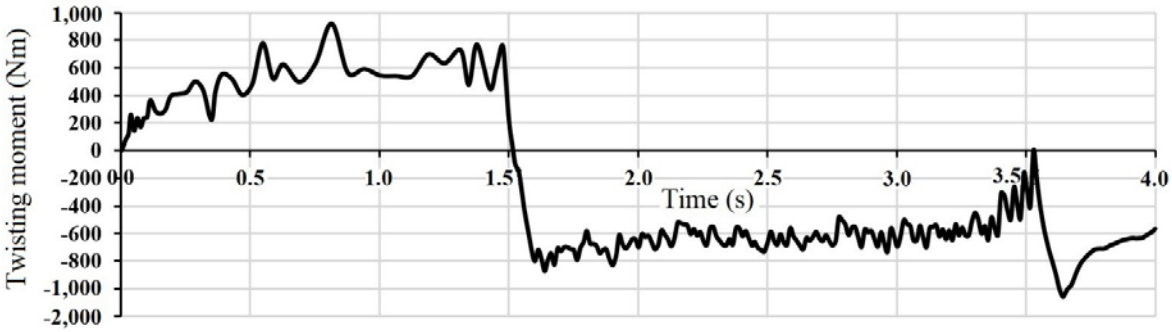

Figure 10. Variation in the total twisting moment during the event.

4.3.3.2 Second step: tension checks and main blade drive

This section presents a different analysis from that presented in step 1, using the same model with the same scale factor for sliding contact penalty. The boundary conditions were prescribed in the form of sinusoidal displacements (f = 40 Hz), with an amplitude of 3 mm to be applied to parts 9 and 11 of the parallel C beams model [Figure 11(a)].

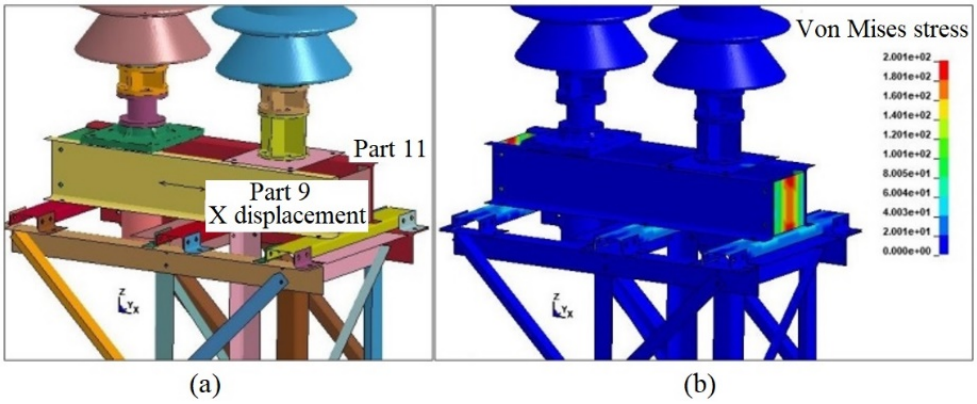

Figure 11. (a) Displacement prescribed for parts 9 and 11. (b) Von Mises stress.

The Von Mises stresses generated by the action of the prescribed displacement are shown in Figure 11(b) for the event time of 0.00625 s, and they have a maximum value of 200 MPa.

The displacement at node 236.371 along the event is shown in Figure 12. In the time of 0.00625 s, the displacement value was 1.48 mm.

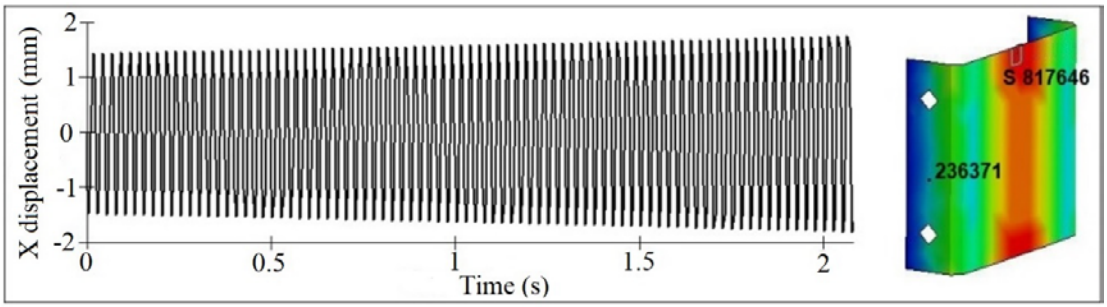

Figure 12. Displacement at node 236,371.

4.3.3.3 Third step: stress checks with other software

To check the stress values observed in the second step in Figure 11(b), a third analysis was carried out only of plate C where the maximum stresses occur using the displacement conditions generated by the sinusoidal load shown in Figure 12. The analysis was static, with the same material used in the second analysis, a kinematic plastic material with a yield stress of 250 MPa, a tangent modulus of 1450 MPa, Poisson's coefficient of 0.3, and elasticity module of 200 GPa (low carbon steel). The boundary conditions, displacements, and Von Mises stresses are shown in Figure 13(a–c), respectively.

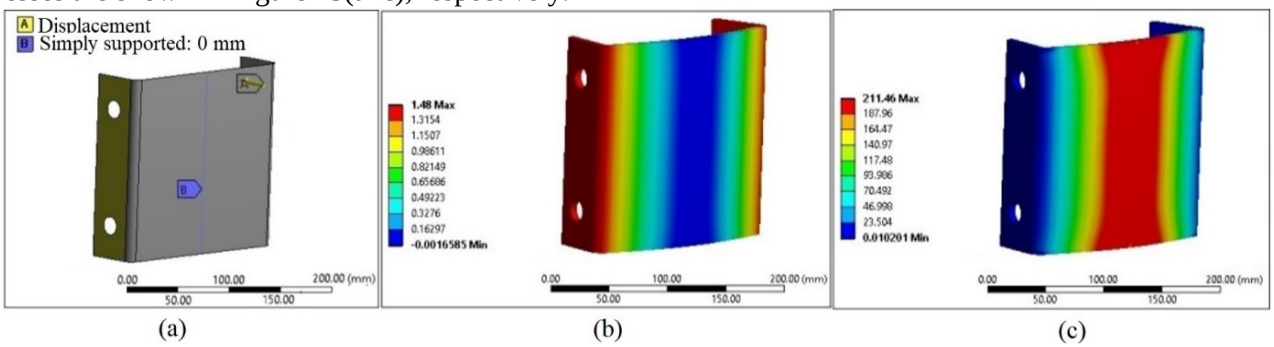

Figure 13. (a) Boundary conditions. (b) Displacements. (c) Von Mises stress.

By comparing the values obtained in the second stage, a Von Mises stress of 200.1 MPa was observed, and the value obtained in the static analysis of the third stage was 211.46 MPa, which is a small difference of 5.67%. Thus, the disconnector model is considered, from the point of view of numerical analysis, calibrated.

4.4 Experimental test: measurement of natural frequencies

4.4.1 Methodology for carrying out the test

Three accelerometers were attached to the end of the main blade, close to the electrical contact, positioned with the axes in the x direction (400 g parallel to the impact, direction of closure of the main blade), in the z direction (100 g vertical), and in the y direction (50 g transversal) [Figure 14(a)].

Figure 14. (a) Accelerometer position. (b) Experimental station and equipment.

The signal acquisition rate was 24,000 Hz using 10,000 points to represent the signal clipping during the impact time.

The data acquisition system used was the ADS 1800, a data acquisition system with 22 bits of resolution and universal input manufactured by Lynx Technologic Electronic [Figure 14(b)]. The following accelerometers were used: 1) model 2220-050, serial 31219, part 153-00098-03 Idd 7.5 mV, bias 8.4 mV, scale factor 79.49 mV/g; 2) model 2210-100, serial 31041, part 153-00097-04, Idd 8.3 mA, bias –1.3 mV, scale factor 40.08 mV/g; 3) model 2210-400, serial 26675, part 153-00097-10, Idd 7.6 mA, bias –5.3 mV, scale factor 10.01 mV/g, each supplied by Silicon Designs Inc. With a steel hammer impacting the center of the main blade, the excitation was obtained, which was measured.

4.4.2 Signals obtained and natural frequencies generated

Natural frequencies were obtained using Matlab software and applying a fast Fourier transform (FFT) generation subroutine. Figure 15 shows the shape of the signals obtained by the impact of the hammer.

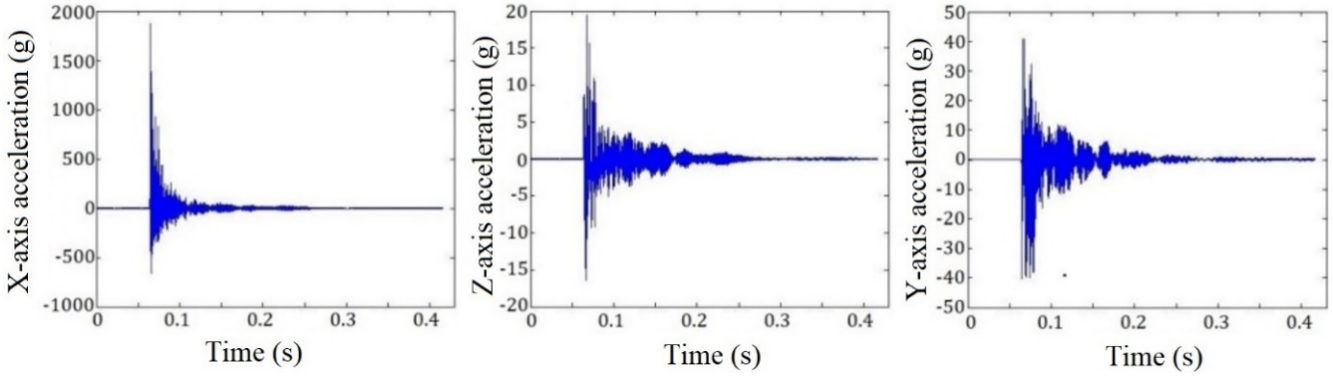

Figure 15. Signs obtained with the impact of the hammer in the centre of the vertical blade.

Figure 16 shows the magnitudes of the accelerations in the frequency domain for the vertical, transverse, and longitudinal directions, with a cut-off at 45 Hz.

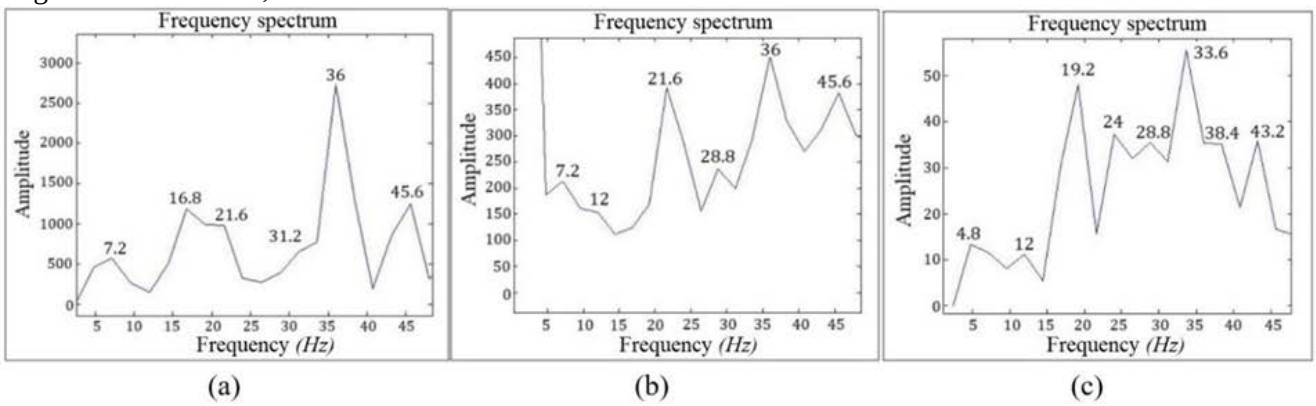

Figure 16. (a) Natural frequencies (x-axis accelerometer and parallel to the impact). (b) Natural frequencies (y-axis accelerometer and transverse to the impact). (c) Natural frequencies (z-axis and vertical accelerometer).

Figure 17 shows the natural frequencies for the first eight modes of vibration obtained using Ansys Ls-dyna software.

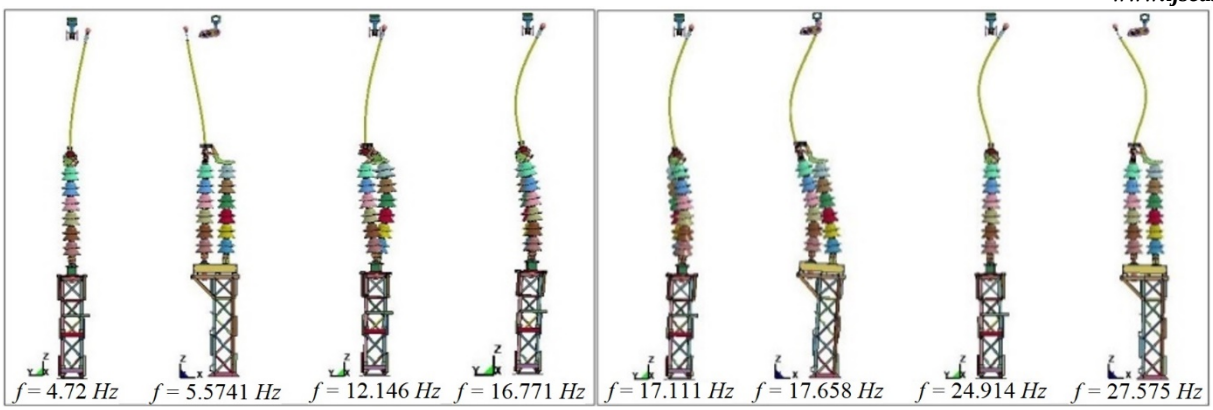

Figure 17. First eight modes of vibration.

Table 2 presents the frequencies obtained in the tests, placed in ascending order, and a comparison between the results obtained experimentally with those obtained by the FEM up to the 12th mode of vibration. The frequencies below the equipment's acquisition capacity (below 4 Hz) were neglected.

Table 2: Natural frequencies (experimental × FEM).

Vibration mode	*Experimental (Hz)*	*FEM (Hz)*	*Difference (%)*
1º	4.8	4.72	2%
2º	7.2	5.57	23%
3º	12	12.14	–1%
4º	16.8	16.77	0%
5º	19.2	17.11	10.9%
6º	21.6	17.65	18.3%
7º	24	24.91	–3.8%
8º	26.4	27.57	–4.4%
9º	28.8	30.42	–5.6%
10º	31.2	32.12	–2.9%
11º	33.6	33.29	0.9%
12º	36	36.18	–0.5%

5. Results and discussion

This section presents the evaluation of the closure of the electrical contact of the vertical reverse disconnector and the stresses under its structure resulting from the action of displacement of the variable amplitude value (1.5 mm, 2 mm, 3 mm) prescribed in a sinusoidal manner (Figure 18) at frequencies of 5 Hz, 10 Hz, 20 Hz, 40 Hz, and 80 Hz applied to the base of the disconnector in profile C, simulating the action of the motovibrator. Through experimental tests, Rocha [1] found that the frequency of 87 Hz significantly reduced the twisting moment required for closing the contact of the double side opening disconnector. In this work, the analyses were carried out with an open electrical contact and an arbitrated distance (this distance varies with each failure closing event) between the mobile and the fixed contact of 63 mm, as shown in detail in Figure 1(c). Displacement ranges were prescribed for the two parallel C beams [part 9 and part 11 in the model in Figure 11(a)]. The best results in terms of closing the electrical contact occurred for the amplitude of 3 mm.

Figure 18 shows the output displacements (sinusoidal curve with amplitude of 3 mm for f=20 Hz) of the software, proving the correct use of the input data in the program and, consequently, the correct prescription of the upper limits of time in the implicit analysis performed. The input curve was generated with 2,560 points and a time step of 1.5625×E–3. The analysis was performed with an upper time limit step of $6.25\times E^{-3}$, which is sufficient for the representation of the curve with at least 3 points every quarter of the period. The same procedure was used for the other frequencies.

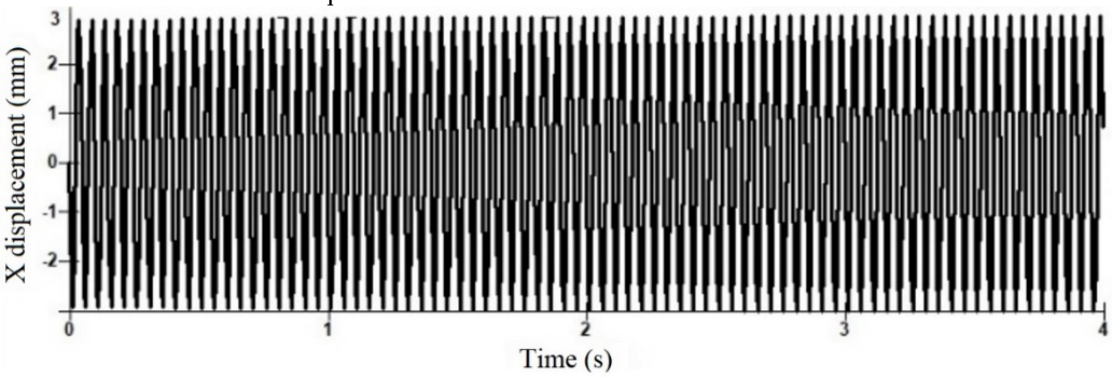

Figure 18. Output curve of the prescribed displacements (f =20 Hz).

Figure 19 shows the maximum displacement obtained for the frequencies of 5 Hz (77.7 mm, t=7.16 s), 10 Hz (182 mm, t=3.28 s), 20 Hz (112 mm, t=1.49 s), 40 Hz (93.7 mm, t=0.072 s), and 80 Hz (273 mm, t=2.45 s), with an amplitude of 3 mm. Regarding the time required for vibration to reach the closing of the electrical contacts, a reduction in the time required to obtain the maximum displacement was observed from 7.16 s to 5 Hz, 3.28 s to 10 Hz, 1.49 s to 20 Hz, and 0.072 s to 40 Hz, which is an average reduction of 1.4 s every time the frequency doubles. For the frequency of 80 Hz, different behavior was observed for the time of 2.45 s, with a strong impact on the electrical contacts. For all frequencies analyzed, the movement of the main blade and the electrical contact occurred suddenly, with a shock against the electrical contacts [Figure 20(a–b)].

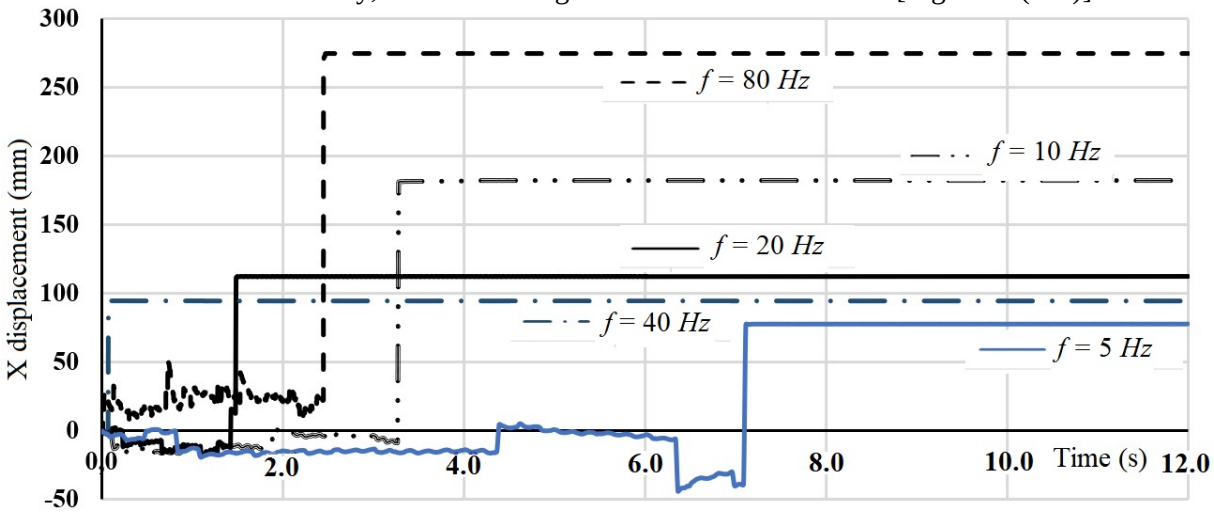

Figure 19. Main blade displacements f = 5, 10, 20, 40, and 80 Hz and amplitude of 3 mm.

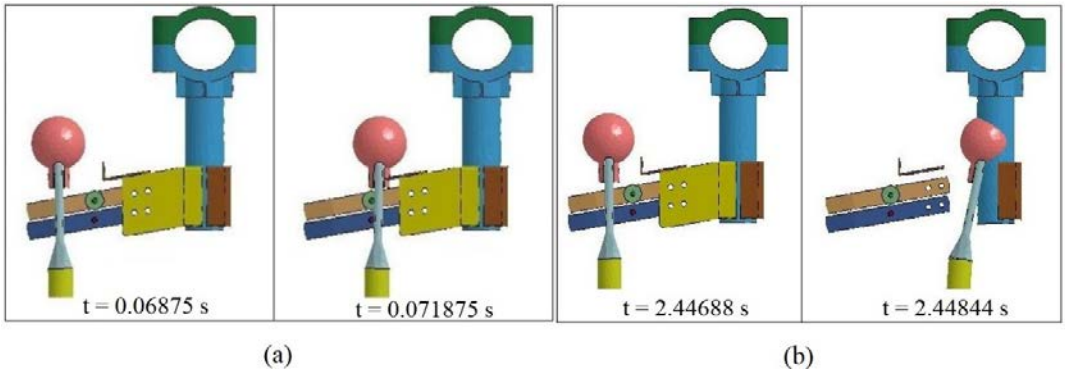

Figure 20. Impact on electrical contact. (a) f = 40 Hz and (b) f = 80 Hz.

Figure 21 shows the displacements of the main blade for the frequency of 5 Hz which amplitude that assumes values of 1.5 mm, 2 mm, and 3 mm. As the amplitude increases, the displacement value increases. Only with a width of 3 mm can a displacement of greater than 63 mm (arbitrated value) be achieved [Figure 1(c)], which is necessary to close the contact. Note that for cases of a possible opening distance between the fixed and mobile contact of less than 30 mm, the contacts would be closed with smaller amplitudes.

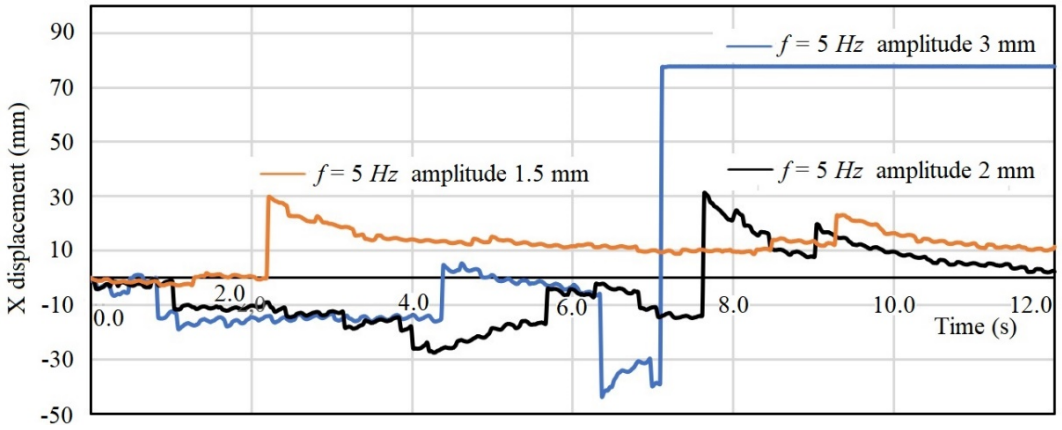

Figure 21. Main blade displacements (f = 5 Hz and amplitudes of 1.5 mm, 2 mm, and 3 mm).

Figure 22 presents the Von Mises stress values (f = 20 Hz, amplitude of 3 mm), shown in red on the side plate of the base C beams, with a maximum value of 195 MPa which is below the yield stress limit of 250 MPa for the material. Considering that the disconnector opening and closing maneuver eventually occurs, fatigue problems are not evaluated. Since the stress values do not depend on the frequency but rather on the prescribed displacement, similar stress values were obtained for the analyses with the other frequencies.

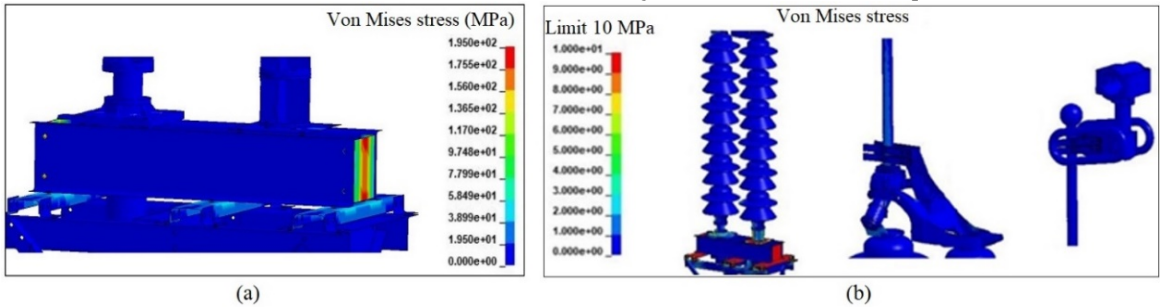

Figure 22. Von Mises stress (a) Base and (b) insulator column, main blade, and contacts.

The Von Mises stresses acting on the insulators, main blade drive mechanism, and fixed and movable contacts are shown in Figure 22(b) for the frequency of 20 Hz and amplitude of 3 mm, with a cut-off point (upper limit) of 10 MPa and very low values, indicating that these components are under low stress requirements.

A simulation of the rotational movement of the main blade, as shown in Figure 9 (prescribed rotation), added to the prescribed vibrational movement through sinusoidal displacement in the x direction with an amplitude of 3 mm applied to the two C beams of the base, as shown in Figure 11(a), producing twisting moments in Figure 23.

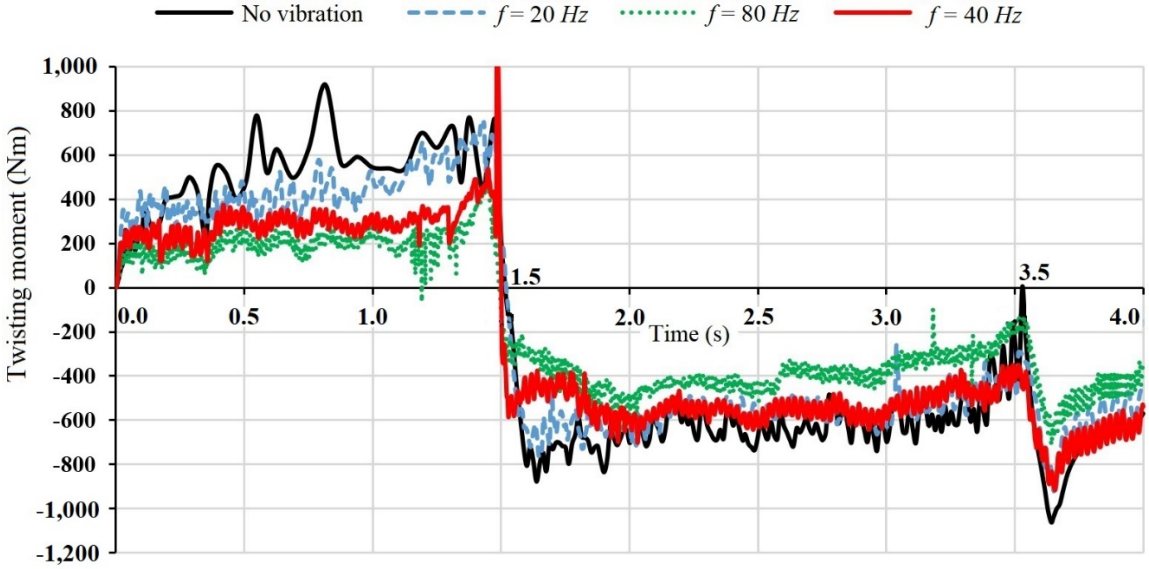

Figure 23. Variation in the twisting moment during the event.

Figure 23 shows that the twisting moment requirement for opening and closing electrical contacts (according to Figure 9) decreases from the non-vibrational situation to the vibrational situation with frequencies of 20 Hz, 40 Hz, and 80 Hz, a reduction in the requirement of twisting moment greater than 50% in the event of opening of the main blade and around 30% in the closing event for the frequency of 80 Hz. This reduction is attributed to the effect of the vibration prescription during the entire time of the event, a fact that has already verified by Rocha [1] through experimental measurements.

The Von Mises stresses generated during the event are shown in Figure 24 (red). The maximum stress value found in the analysis was 170 MPa (below the yield stress of the material, which is 250 MPa), which occurred on the connection plate of the C profiles of the disconnector base. It is concluded that the application of vibration throughout the opening and closing event of the main blade has an effect of reducing the twisting moment requirements and facilitating the opening and closing of the electrical contact.

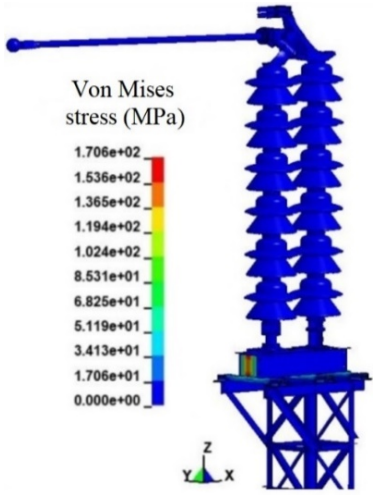

Figure 24. Main blade opening and closing stresses (f = 80 Hz).

6. Conclusion

The vibration generated by the motovibrator on the structure of the vertical reverse disconnector under study with frequencies of 5 Hz, 10 Hz, 20 Hz, 40 Hz, and 80 Hz and prescribed displacement amplitudes of up to 3 mm produce displacement values of the main blade that lead to closing of the electrical contact. Lower frequency values (5 Hz, 10 Hz, and 20 Hz) produce better results, with a moderate impact on the electrical contacts. Higher frequency values (40 Hz, 80 Hz) have a very strong impact, causing damage to the electrical contacts. The lower the frequency, the longer the time required to generate the displacement required to close the electrical contacts.

The amplitude of the sinusoidal displacement value prescribed at the base of the disconnector influences the displacement of the main blade (greater amplitudes, greater displacements).

The values of stresses, resulting from the vibration of the structure and the sinusoidal displacements prescribed in the base, are below the yield stress of the materials used in the structure of the sub-base, base, insulator columns, drive mechanisms, and main blade and contacts, not representing risk of failure for the disconnector.

As already demonstrated experimentally by Rocha [1], the twisting moment required for the disconnector to operate decreases with the increase in the activation frequency with a reduction of up to 50% for the frequency of 80 Hz.

Acknowledgments

The authors are grateful for the financial support of the State Electricity Generation and Transmission Company (CEEE-GT) through the Research and Development Program of the National Electric Energy Agencies (ANEEL) under contract No. 9953349, as well as the institutional support of Passo Fundo Foundation University (FUPF).

References

[1] Rocha LF. Development of a system for maneuvering high voltage disconnectors aiming at its automation process [Dissertation]: University of Passo Fundo; 2014 (in Portuguese).
[2] Rocha LF. Inventor; CEEE, Assignee; FUPF, Assignee. High voltage disconnect automation device. Brazil BR 1020130201987, 2013.
[3] Gedra RL, Barros BF, Borelli R. Electricity generation, transmission, distribution and consumption. São Paulo: Érica, 2014 (in Portuguese).
[4] Carrasco AC, Torres GL. Intelligent system for the detection of manoeuvre failures in power substation disconnectors. Exact Sciences Magazine, São Paulo, 2005 (in Portuguese).
[5] Mosalam KM, Gunay S. Seismic performance evaluation of high voltage disconnect switches using real-time hybrid simulation I: system development and validation. Earthquake Engineering and Structural Dynamics, 2014; 43:1205-1222.
[6] Mosalam KM, Gunay S. Seismic performance evaluation of high voltage disconnect switches using real-time hybrid simulation II: parametric study. Earthquake Engineering and Structural Dynamics, 2014; 43: 1223-1237.
[7] Semedo SMV, Oliveira EGJ, Cardoso FJA. Remote monitoring of high voltage disconnect switches in electrical distributions substations. IEEE 23rd International Symposium of Industrial Electronics (ISIE), 2014.
[8] Zangl H, Bretterklieber T, Brasseur G. A feasibility study on autonomous online condition monitoring of high-voltage overhead power lines. IEEE Transactions on Instrumentation and Measurement, Vol. 58, no.5, may 2009: 1789-1796.
[9] Galin M, Visan G, Ioan T. P. Electric and magnetic field distribution inside high voltage power substations. Numerical modeling and experimental measurements. IEEJ Trans 2010; 5:40–5.
[10] Brazilian Association of Technical Standards. NBR 7571 – Disconnectors: technical and dimensional characteristics, 2011 (in Portuguese).
[11] Souza A. F. System for monitoring the operation of high voltage disconnect switches based on the analysis of the drive motor chains [Dissertation]: Federal University of Santa Catarina; 2002 (in Portuguese).
[12] Brazilian Association of Technical Standards. IEC/TR 60943 Guidance concerning the permissible temperature rise for parts of electrical equipment, in particular for terminals, 2009.
[13] Macedo E. Noise from electric power transmission lines. Angola Power Services: 2011. Available from: http://angolapowerservices.blogspot.com/2011/02/ruido-das-linhas-de-transmissao-de.html. Accessed in Aug. 2018.
[14] Hibbeler R. C. Dynamics: mechanics for engineering. 12th edition. São Paulo: Pearson Prentice Hall; 2011 (in Portuguese).
[15] Thomson WT. Vibration theory. Rio de Janeiro: 12/5000 Interscience; 1978 (in Portuguese).
[16] Rao SS. Mechanical vibrations. 5th edition. Upper Saddle River: Prentice Hall; 2011.
[17] Alves Filho A. Finite elements: dynamic analysis. 2nd edition. São Paulo: Érica; 2008 (in Portuguese).
[18] Zienkiewicz O. C., Taylor R.L. The finite element method. 4th. London: McGraw-Hill; 1989.
[19] LSTC, Livermore Software Technology Corporation. Ls-dyna – Keyword User`s Manual. Version 970. LSTC: Califórnia, 2003.
[20] Bathe K. J. Finite element procedures. Englewood Cliffs, New Jersey: Prentice Hall; 1996.
[21] Cook D. R, Malkus D.S., Plesha E. M. Concepts and applications of finite element analysis. John Wiley & Sons; 1988.
[22] LS-DYNA. User Manual – Non-linear Dynamic Analysis of Structures. Version 950-d Livermore Software Technology Corporation 7374. Las Pocitas Road Livermore, 1999.
[23] ANSYS, Inc. Theory Manual. Release 5.7. 0011369. Twelfth Edition. SAS IP, Inc., 1984.
[24] Grimes R. G, Lewis J. G., Simon H. D. A shifted block Lanczos algorithm for solving sparse symmetric generalized eigenproblems. SIAM Journal on Matrix Analysis Applications 1996;1.

[25] Rajakumar C., Rogers C. R. The Lanczos algorithm applied to unsymmetric generalized eigenvalue problems. International Journal for Numerical Method in Engineering 1991; 32.
[26] Lingling L. I. et al. An integrated approach of reverse engineering aided remanufacturing process for worn components. Robotics and Computer-Integrated Manufacturing 2017;48.
[27] Poel Filho C, et al. Importance of reverse engineering for modernization reforms of hydroelectric plants and their equipment. XXIII National Seminar on Electric Energy Production and Transmission SNPTEE, Brazil, 2015 (in Portuguese).
[28] Weimar, Klaus (Compiled). Ls-Dyna – User's Guide. Rev. 1.19. PWS e CAD-FEM GmbH: 2001.

Me. Maira Duarte Mores
Degrees achieved: Master's in mechanical Engineer (Projects and Manufacturing Processes, University of Passo Fundo, Passo Fundo, Rio Grande do Sul, Brazil, 2020); Post-graduated in Mathematics (University of Passo Fundo, Passo Fundo, Rio Grande do Sul, Brazil, 2006); Mechanical Engineer (University of Passo Fundo, Passo Fundo, Rio Grande do Sul, Brazil, 2010); Degree in Mathematics and Physics (Integrated Regional University, Erechim, Rio Grande do Sul, Brazil, 2003). **Current Employment**: Businesswoman and Commercial Representative (ALM Distributional, Erechim, Rio Grande do Sul, since 07/2019); Budgetist (Metalúrgica NovaJVA, Marau, Rio Grande do Sul, (period 2013 and 2014); Mechanical Engineer / Contracts Coordinator / Designer / Purchaser (Intecnial Metalúrgica, Erechim, Rio Grande do Sul, period 2006 to 2012). **Major academic achievements:** Mathematics Professor in Environmental Engineering, Agronomy and Licentiate Courses (Federal University Frontier South, Rio Grande do Sul, Erechim (period 2014 to 2015).

Dr. Agenor Dias de Meira Junior
Degrees achieved: MBA in Management of Higher Education Institutions (University of Caxias do Sul, Caxias do Sul, Rio Grande do Sul, Brazil, 2017); PhD in Engineering (Federal University of Rio Grande do Sul, Brazil, 2010); Master in Mechanical Engineering (Federal University of Santa Catarina, Santa Catarina, Brazil, 1994); Civil Engineer (Passo Fundo University, Passo Fundo, Rio Grande do Sul, 1998); Mechanical Engineer (Federal University of Rio Grande do Sul, Santa Maria, Rio Grande do Sul, Brazil, 1998). **Current Employment**: Professor of the Mechanical Engineering Course and the Master Program in Design and Manufacturing Processes at the University of Passo Fundo (Passo Fundo, Rio Grande do Sul, Brazil). **Major academic achievements**: Administrative Vice-Rector of the University of Passo Fundo (Passo Fundo, Rio Grande do Sul, Brazil, period 2010-2018); Principal of the Faculty of Engineering and Architecture of the University of Passo Fundo (Period 1998-2002); Researcher at the Master Program in Design and Manufacturing Processes (PPGPPF) at the University of Passo Fundo (since 2010) developing research in the areas of mechanics of solids and numerical methods.